NATIONAL ADVISORY COMMITTEE FOR AERONAUTICS

TECHNICAL NOTE 3688

STATIC-THRUST MEASUREMENTS OF THE AERODYNAMIC LOADING ON A HELICOPTER ROTOR BLADE

By John P. Rabbott, Jr.

Langley Aeronautical Laboratory
Langley Field, Va.

Washington
July 1956

NATIONAL ADVISORY COMMITTEE FOR AERONAUTICS

TECHNICAL NOTE 3688

STATIC-THRUST MEASUREMENTS OF THE AERODYNAMIC LOADING ON A HELICOPTER ROTOR BLADE

By John P. Rabbott, Jr.

SUMMARY

An experimental investigation of the aerodynamic loading on a 15-foot-diameter helicopter rotor blade in static thrust was conducted for a tip-speed range of 400 to 500 feet per second and disk loads of zero to about 2.5 pounds per square foot. The chordwise pressure distributions at five spanwise stations are presented and a comparison is made between the measured spanwise loading and a simple theoretical loading modified by an approximate correction for a finite number of blades.

The variation of spanwise load distribution near the blade tip with thrust indicates that the blade tip loss is proportional to the thrust coefficient.

INTRODUCTION

Because of the very complex flow pattern in a helicopter-rotor wake, the calculation of the aerodynamic loading on a rotor blade is a difficult mathematical problem whose solution is possible only when many simplifying assumptions as to the distribution of induced velocity across the rotor disk are made.

The total thrust of a rotor, when calculated from blade-element strip analysis and modified by a suitable tip-loss factor, has been found to agree fairly well with the actual thrust. However, very little experimental data have been available heretofore to compare with the calculated spanwise distribution of loading. Reference 1 is an experimental investigation of the aerodynamic loading on a model rotor blade for a wide variety of flight conditions, but it is limited somewhat by the relatively low frequency response of the pressure measuring equipment in forward flight. For the static-thrust condition, reference 1 presents the chordwise and spanwise loading on a rotor blade at one pitch angle and one tip speed.

The present report presents the static-thrust portion of the results of an investigation to measure the dynamic rotor-blade loading for a series of flight conditions from static thrust through forward flight. Chordwise pressure distributions at five spanwise locations were measured for a range of pitch angles from slightly negative to a value corresponding to maximum allowable design load on the blade, a disk loading of about 2.5 pounds per square foot, for tip speeds of 400 to 500 feet per second. These data are presented and a comparison is made with a theoretical spanwise loading. Some discussion of an appropriate tip-loss factor to be used in the theoretical performance calculations is given also.

Simultaneous measurements of rotor thrust and torque input were also made and are presented.

SYMBOLS

A_f area of fuselage immersed in rotor wake, sq ft

B tip-loss factor, $1 - \frac{\sqrt{2C_T}}{b}$; blade elements outboard of radius BR are assumed to have profile drag but no lift

b number of blades

C_D vertical drag coefficient of fuselage, $\frac{\text{Fuselage drag}}{\frac{\rho}{2}v_f^2 A_f}$

C_l section lift coefficient, Lift/qc

C_T thrust coefficient, $\frac{T}{\pi R^2 \rho(\Omega R)^2}$

$C_{T,c}$ corrected thrust coefficient from wind-tunnel balance

$C_{T,m}$ measured thrust coefficient from wind-tunnel balance

C_Q rotor-shaft torque coefficient, $\frac{Q}{\pi R^2 \rho(\Omega R)^2 R}$

c blade-section chord, ft

Q rotor-shaft torque, lb-ft

q local dynamic pressure, $\frac{\rho}{2}(r\Omega)^2$

R blade radius measured from center of rotation, ft

r radial distance to blade element, ft

T rotor thrust, lb

T_m measured rotor thrust from wind-tunnel balance, lb

v_f value of rotor-induced velocity at fuselage, taken as induced velocity in ultimate wake, $\Omega R\sqrt{2C_T}$, ft/sec

x distance from leading edge to any point on chord, ft

θ blade-section pitch angle, deg

ρ mass density of air, slugs/cu ft

σ rotor solidity, $bc/\pi R$

Ω rotor angular velocity, radians/sec

EQUIPMENT AND TESTS

The rotor blades are of rectangular, untwisted plan form with a 15-foot diameter, an NACA 0012 airfoil section, and a rotor solidity of 0.097. One blade of the two-bladed teetering rotor was instrumented with NACA miniature electrical pressure gages (ref. 2) to measure the differential pressures of the upper to the lower surface at ten chordwise locations for each of five spanwise stations. The uninstrumented blade has a very slightly greater thickness than the instrumented blade, as some additional layers of covering material were added for balance. Figure 1 is a sketch of the instrumented rotor blade showing the principal dimensions and the pressure-orifice locations, and figure 2 is a photograph of a section of the instrumented blade taken during its construction. This figure shows the location of the pressure gages and the associated wiring and tubing. The wires to the gages were imbedded in the surface of the blade and led to a terminal strip at the root where connection to the hub and slip rings was made. The forward portion of the blade, from the leading edge to the quarter chord, was formed of an aluminum D-section spar covered with balsa fairing strips. The rear portion was built up of plywood ribs and balsa planking, and the whole blade was then covered with one layer of fiber glass impregnated with Paraplex resin.

A 7-inch length of Monel tubing with an inside diameter of 0.060 inch was used to connect both the upper- and the lower-surface orifices to the corresponding pressure gage. This dimension was kept constant for all pressure pickups so that the frequency response and phase shift would be the same for all gages. Figure 3 shows the frequency-response characteristics for a typical gage and tubing combination. For the highest rotational speed tested, the installation gave a flat frequency response through the sixth harmonic.

Although forty-five slip rings were available for electrical connection between the rotating and stationary parts of the model, this number was not sufficient to enable all five stations to be recorded at one time. Therefore, a remotely operated stepping switch located on the rotor hub was employed whereby stations 1, 2, and 3 (at 0.31, 0.56, and 0.75 radius) were recorded simultaneously. The switch was then advanced and stations 3, 4, and 5 (at 0.75, 0.85, and 0.95 radius) were recorded. Station 3 was thus repeated at each test point as a check on the repeatability of the data.

Figure 11 of reference 2 shows a circuit diagram essentially the same as the one used for this investigation. The NACA miniature electrical pressure gages formed two arms of a four-arm bridge circuit, the other two being a dummy half-bridge. In order to eliminate interaction between gages, since a common power lead was used for each station, the circuit used herein employed a 1:1 transformer for the dummy half-bridge, rather than the 25-ohm resistors shown in reference 2. These transformers were also installed on the top of the rotor hub, between the gage output and the slip rings.

The model was mounted in the open-throat test section of the Langley full-scale tunnel to enable the use of the wind-tunnel balance to measure the total rotor thrust. Figure 4 shows the model in operation in the tunnel. The rotor forces were transmitted by the struts on which the model was mounted to the balance below. A strain gage located on the rotor shaft measured the torque input.

Tests were conducted at tip speeds of 402, 452, and 496 ft/sec for a range of blade pitch angles from slightly negative to a value giving approximately 500 pounds of thrust. These conditions correspond to rotor mean lift coefficients of 0.26 to 0.40. For each condition, oscillograph records of the output of each pressure gage were taken, along with the rotor thrust from the tunnel balance and the torque input.

CORRECTIONS TO DATA

Since no oscillating loads were measured, as is expected in static thrust, there were no amplitude or phase-angle corrections to the pressure

data; however, the rotor thrust as measured on the wind-tunnel balance did require a correction. The balance read the net thrust, or lift force, on the model as a whole; but, since the rotor induced velocity impinged on the fuselage and created a down load, the true rotor thrust was the balance reading plus an amount equal to the down load or the vertical drag on the fuselage. In order to obtain the fuselage drag coefficient, since the fuselage had an irregular shape, a 1/15-scale model of the fuselage was constructed and tested in a small open-throat wind tunnel with the airstream normal to the horizontal plane of the fuselage. The drag was measured with a small strain-gage balance inside the model, and the drag coefficient obtained thereby was used to compute the down load on the full-scale fuselage. The thrust correction was of the form

$$\Delta T = C_D \frac{\rho}{2} v_f^2 A_f$$

where v_f, the value of the induced velocity at the fuselage, was assumed to be uniform and equal to twice the momentum value at the rotor disk, because the fuselage was one rotor radius below the hub and the rotor wake was taken to be fully contracted within this distance. Therefore,

$v_f = \Omega R \sqrt{2C_T}$ and the corrected thrust coefficient is

$$C_{T,c} = \left[\left(T_m + \Delta T\right)/T_m\right] C_{T,m}$$

The area of the fuselage affected A_f was taken as that part that was within the contracted wake. This thrust correction is of the order of 10 percent of the measured thrust.

A tare correction was applied to the measured torque because of the resistance of the shaft bearings above the torque strain gage and some possible wind resistance of the rotor hub, but this tare was a small percentage of the measured torque in a normal operating range (about 1 percent at a thrust coefficient of 0.005).

RESULTS AND DISCUSSION

Performance Data

Figure 5 represents the static-thrust performance and shows a comparison of the measured balance thrust and torque with the theoretical values and with the rotor thrust as obtained from the integrated pressure data. The two dashed curves are for the theoretically computed thrust and torque, whereas the wind-tunnel-balance thrust and torque data

are represented by the circle and square symbols. The experimental points from the tunnel balance for a tip speed of 402 ft/sec are not plotted in order to keep the figure from being unduly crowded; these points fall in the same pattern as the data for tip speeds of 452 and 496 ft/sec. The two theory curves were obtained from the same blade-element strip analysis but have different tip-loss factors; one is equal to the commonly used $B = 0.97$; the other is equal to $B = 1 - \frac{\sqrt{2C_T}}{b}$ as suggested in reference 3. The latter factor, which is seen to give very good agreement with the measured tunnel-balance data, averaged 0.97 over the range of the tests but gave a greater loss at the higher thrust coefficients. This increase in tip loss with thrust coefficient is shown again later in the spanwise-aerodynamic-loading data.

The solid curve in figure 5 represents a fairing of the integrated pressure data, and the difference between these data and the scale data is entirely attributable to a difference in thrust, since the same torque data were used to plot both. This difference amounts to about 5 percent at a representative thrust coefficient of 0.005 and is possibly due to the aforementioned slight dissymmetry in thickness between the two rotor blades which might result in a different lift on each blade.

When thrust coefficient or torque coefficient is plotted against blade pitch angle, no scale effect is found to be present for the range of rotational speeds covered in this investigation.

Chordwise Loading

Figure 6 shows some representative chordwise pressure distributions for three tip speeds at approximately the same blade pitch angle. The curves are conventional in shape, with the total chordwise loading increasing radially until 0.95 radius is reached; at this point, the loading decreases, as would be expected from consideration of the blade tip loss. An additional characteristic that is noticeable, however, which indicates that this decreased load is not entirely attributable to tip loss, is that the loading near the trailing edge is relatively lower for the outboard station than for those inboard. This is more clearly shown in figure 7 where a comparison is made between the measured loading at two spanwise stations and the theoretical chordwise loading, as obtained from reference 4. Figure 7(a), at 0.75 radius, is representative of the inboard stations and shows good agreement between measurements and theory. At 0.95 radius (fig. 7(b)), however, the measured data are seen to be much lower at the trailing edge than the theory shows. (Since both curves are for the same lift coefficient and because the theoretical values are higher at the trailing edge than the measurements, it follows that the theoretical values must be lower at the leading edge to make the area under both curves the same.) This difference was

originally suspected to be caused by a deviation in blade contour from a true NACA 0012 profile, such as reflex at the trailing edge at those stations or blade twist, but these have been checked and no physical deformities were measurable. Since this effect is found near the blade tip, however, the possibility is suggested that this may be an aerodynamic effect, such as an increase in the boundary layer toward the tip due to rotation effects, which could give the blade an effective negative camber. Without two-dimensional tests of this particular blade, however, this phenomenon cannot be resolved.

An indication of the repeatability of the data is given in figures 6 and 8 by comparison of station 3 (0.75R), where the pressures were recorded twice. The agreement is seen to be quite close for all runs.

Spanwise Loading

Figure 8 is a plot of the spanwise aerodynamic loading for several blade pitch angles at the three tip speeds presented. The peak load is seen to occur at 90 to 95 percent radius and move inboard as the total loading, and therefore the tip loss, increases.

A comparison of the relative loading at stations 4 and 5 (at 0.85R and 0.95R, respectively) for a given tip speed shows that as the loading increases, and therefore the thrust coefficient increases, the tip loss also increases, as is evidenced by a decrease in the magnitude of the loading at 0.95R relative to the next inboard station. This indicates that, in calculating the theoretical performance of a rotor, a tip-loss factor which is proportional to the thrust coefficient is closer to the actual condition than is a constant factor which is normally used. For the range of thrust coefficients covered in this test, the tip-loss factor which was based on thrust coefficient, varied from 0.94 at maximum thrust to 1.0 at zero thrust; the average tip-loss factor was approximately 0.97, a value commonly used when a constant factor is employed.

Figure 9 is a comparison of the measured data with three theoretical curves. The short-dashed curve for blade-element theory is obtained from the strip analysis mentioned in the discussion of performance data and has the same thrust coefficient as the measured data when the tip-loss factor based on thrust coefficient is included. The curve for modified theory is derived from the curve for blade-element theory by applying to it an approximate correction for a finite number of blades developed by Prandtl for a lightly loaded propeller. (See ref. 5.) As seen from the figure, the correction approximates the measured loading near the blade tip fairly well, but the modified theory is still high in the region of 50 percent to 85 percent radius, as the correction has no effect inboard of 80 percent radius.

Figure 9 also shows that the more complicated Goldstein vortex theory for propellers (ref. 6) gives less agreement with the measured data for the static-thrust conditions presented here than does the simple Prandtl correction.

Thus, for performance calculations, use of a tip-loss factor in the strip-analysis theory predicts the total thrust quite well; but, to calculate accurately the spanwise distribution of loading, as would be desired for structural analysis, a procedure different from the simple Prandtl correction to blade-element theory or the more complicated Goldstein theory is required. Possibly this procedure might be based on an empirical correction to the theory derived from the measured data.

CONCLUSIONS

The results of an investigation of the chordwise and spanwise aerodynamic loading measured on a 15-foot-diameter helicopter rotor blade in static thrust for a tip-speed range of 400 to 500 feet per second and disk loads of zero to about 2.5 pounds per square foot lead to the following conclusions:

1. The chordwise pressure distributions are, in general, conventional in shape. However, the loading near the trailing edge of the outboard portion of the rotor is lower than expected from theory or from a comparison of the loading at the inboard stations; perhaps this is due to a spanwise boundary-layer growth adding to the reduction of the total load expected from tip-loss considerations.

2. The spanwise loading increases smoothly from the root toward the tip, with the peak loads occurring at 90 to 95 percent radius and being farther inboard at the higher thrust coefficients; thus, a greater tip loss is indicated at these points.

3. The theoretical spanwise loading obtained from blade-element strip analysis overestimates the actual loading outboard of 50 percent radius. A simple Prandtl correction to this theory for a finite number of blades gives close agreement in the region of the tip but has no effect inboard of 80 percent radius.

4. The distribution of loading near the blade tip indicates that a tip-loss factor to be used in calculating the theoretical rotor performance

from strip analysis should be a function of the thrust coefficient rather than a constant factor as is more commonly used.

Langley Aeronautical Laboratory,
National Advisory Committee for Aeronautics,
Langley Field, Va., February 20, 1956.

REFERENCES

1. Meyer, John R., Jr., and Falabella, Gaetano, Jr.: An Investigation of the Experimental Aerodynamic Loading on a Model Helicopter Rotor Blade. NACA TN 2953, 1953.

2. Patterson, John L.: A Miniature Electrical Pressure Gage Utilizing a Stretched Flat Diaphragm. NACA TN 2659, 1952.

3. Gessow, Alfred, and Myers, Garry C., Jr.: Aerodynamics of the Helicopter. The Macmillan Co., c.1952, p. 73.

4. Abbott, Ira H., von Doenhoff, Albert E., and Stivers, Louis S., Jr.: Summary of Airfoil Data. NACA Rep. 824, 1945.

5. Glauert, H.: Airplane Propellers. Propellers of Highest Efficiency. Vol. IV of Aerodynamic Theory, div. L, ch. VII, sec. 4, W. F. Durand, ed., Julius Springer (Berlin), 1935, pp. 261-269.

6. Goldstein, Sydney: On the Vortex Theory of Screw Propellers. Proc. Roy. Soc. (London), ser. A, vol. 123, no. 792, Apr. 6, 1929, pp. 440-465.

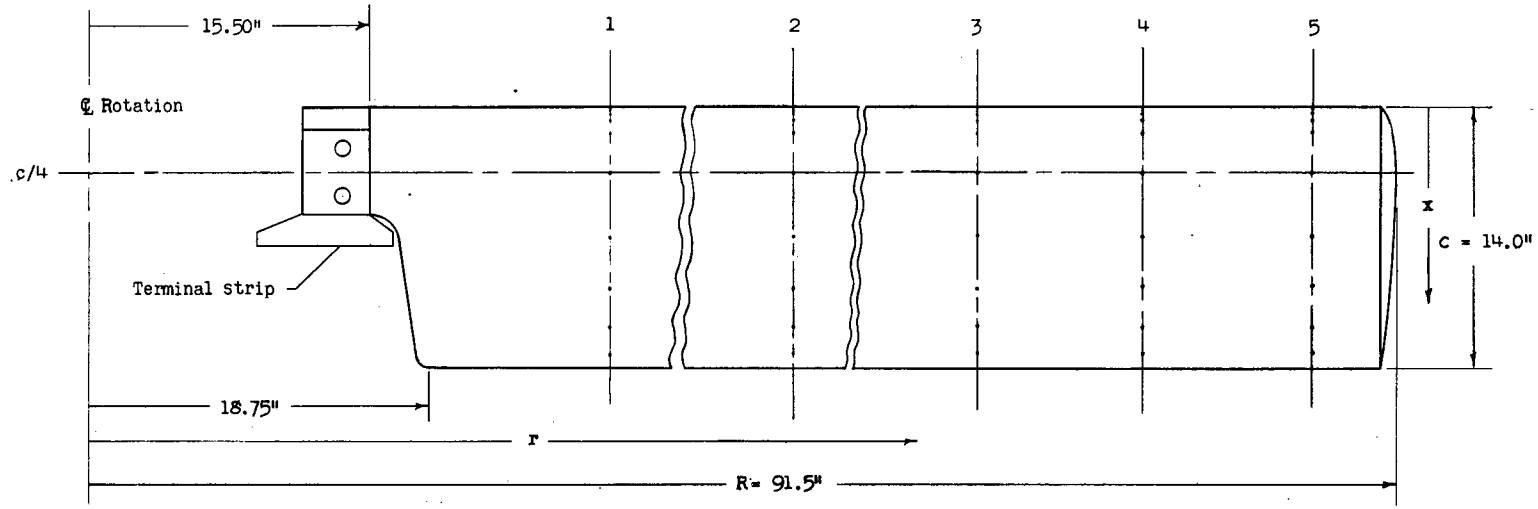

Chordwise station	x/c
1	0.005
2	.010
3	.025
4	.050
5	.100
6	.250
7	.500
8	.700
9	.850
10	.950

Radial station	r/R
1	0.31
2	.56
3	.75
4	.85
5	.95

Figure 1.- Blade layout showing location of pressure orifices. Airfoil section, NACA 0012; rotor solidity $\sigma = 0.097$.

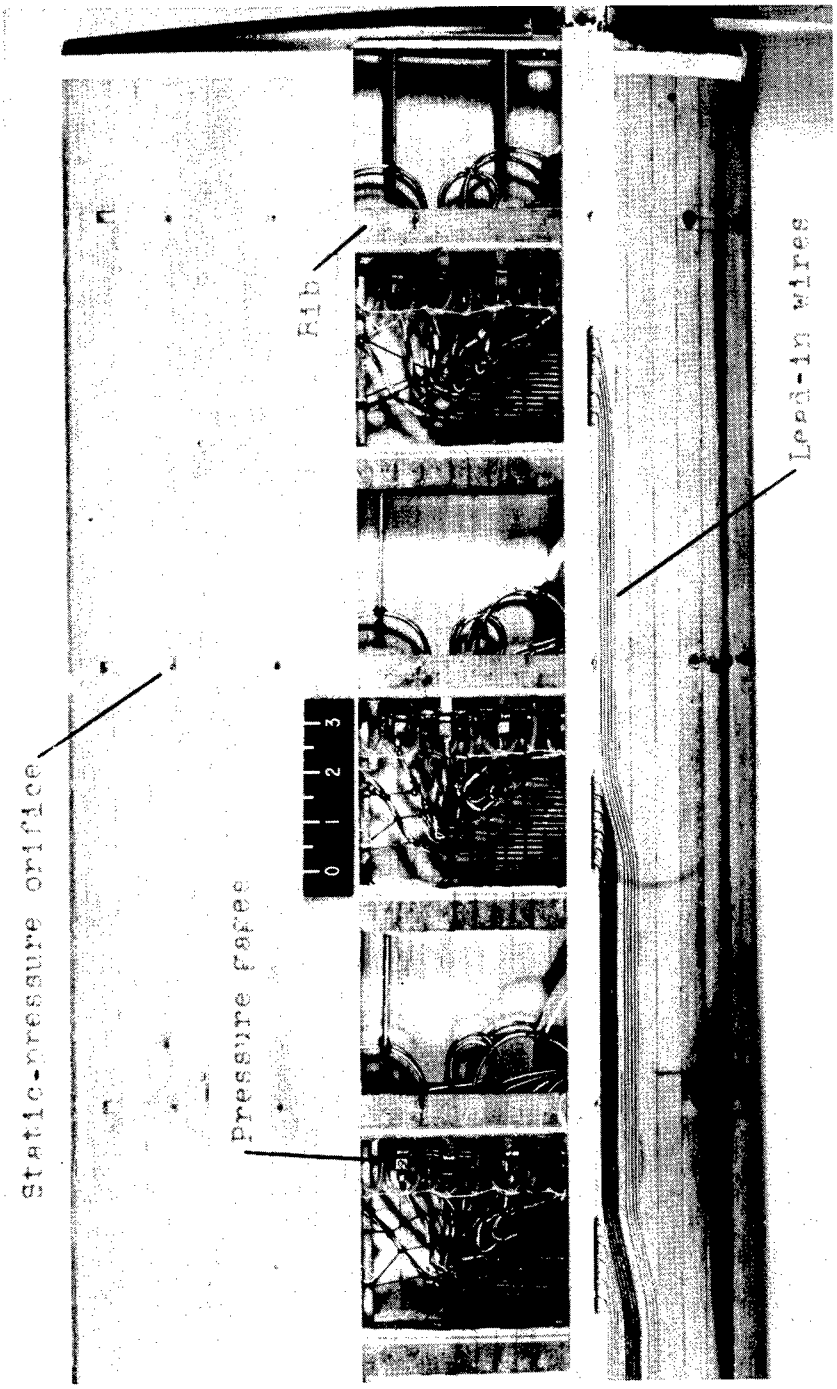

L-83994.1

Figure 2.- Photograph of outer portion of blade showing pressure-gage and wiring installation.

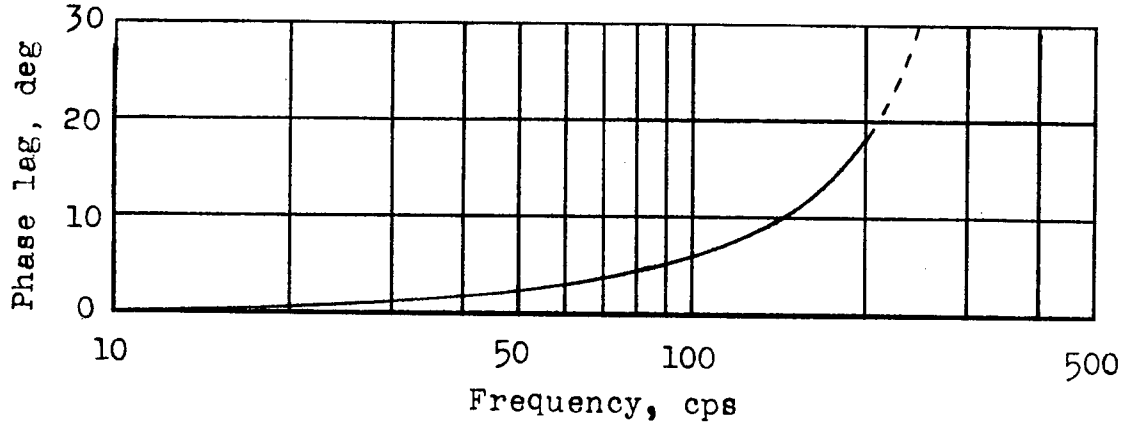

(a) Phase angle.

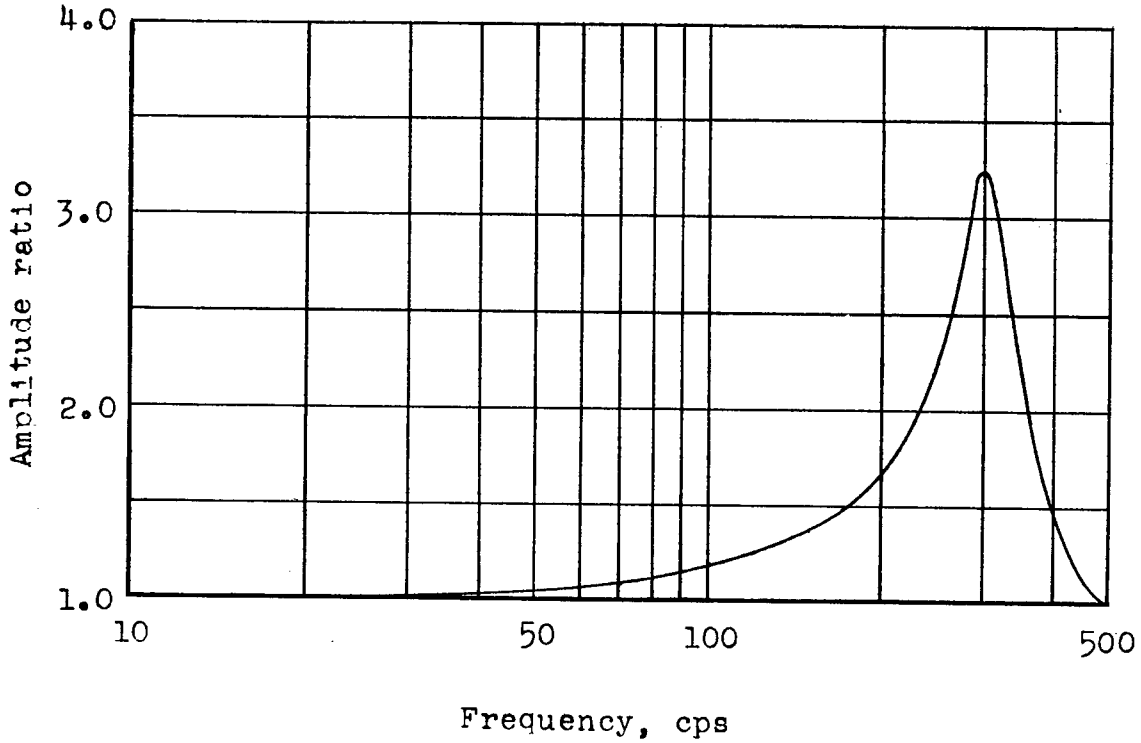

(b) Amplitude ratio.

Figure 3.- Frequency response and phase-lag angle for typical pressure-gage and tubing combination.

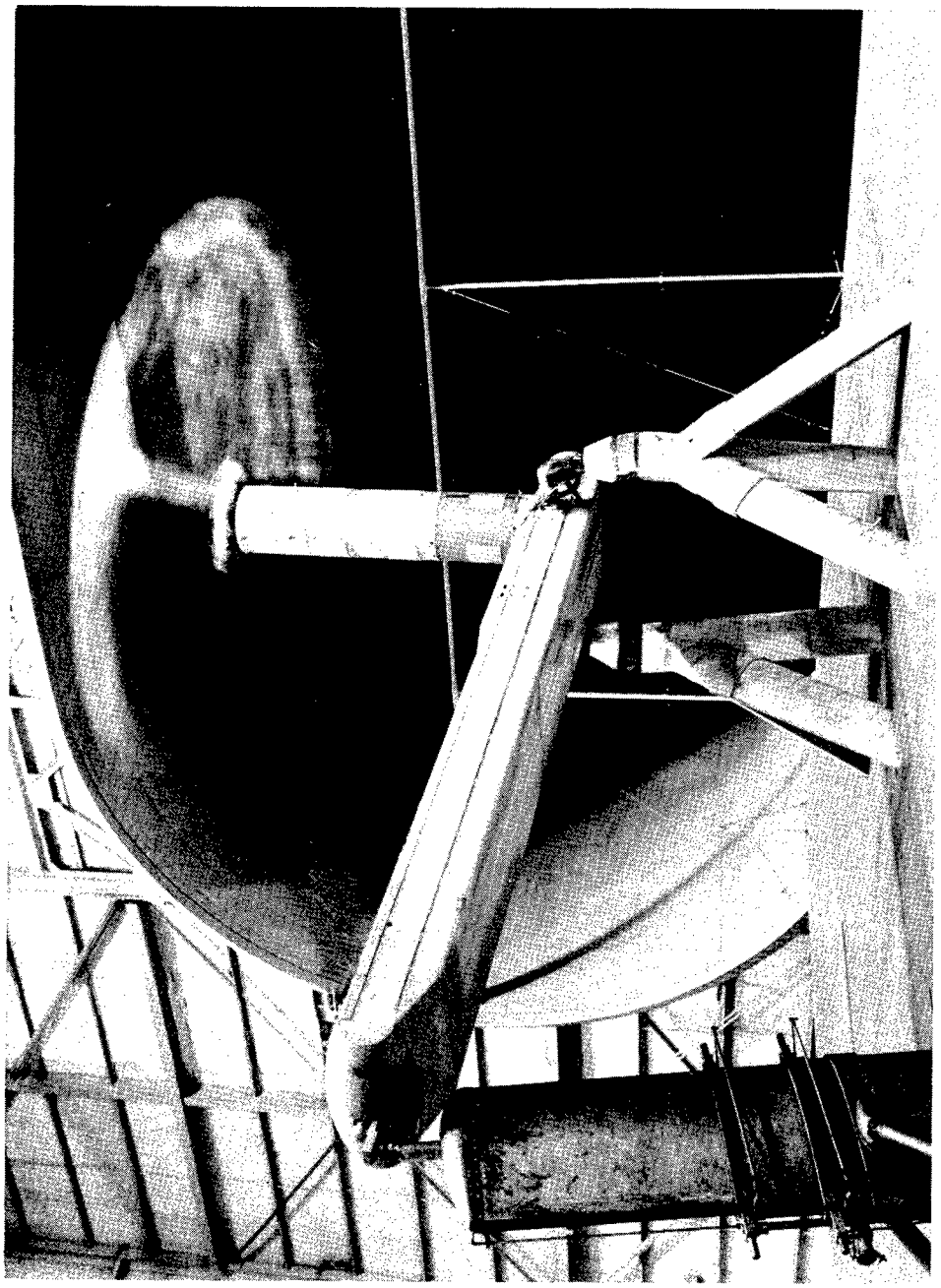

L-83264.1

Figure 4.- General view of model in Langley full-scale tunnel.

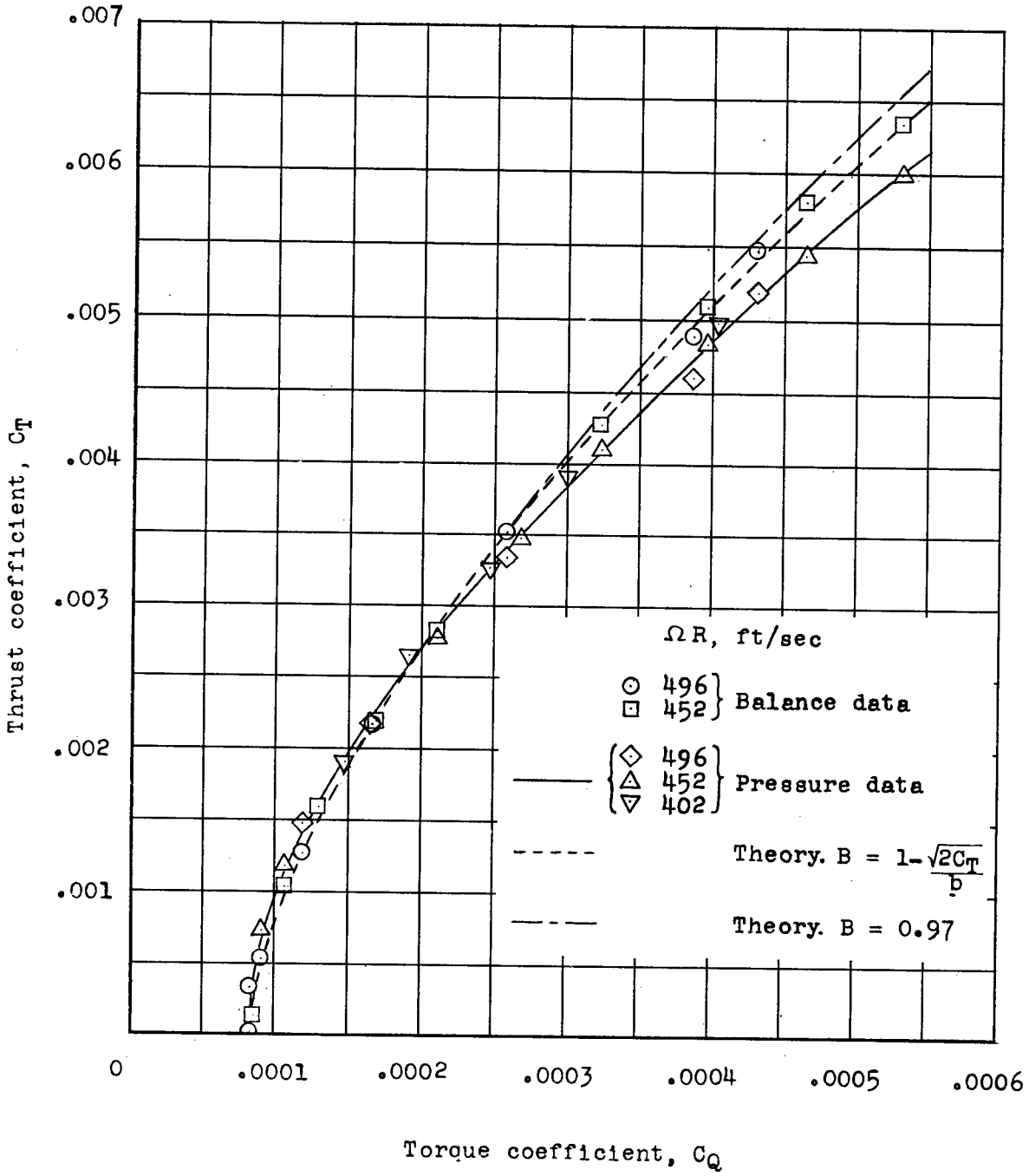

Figure 5.- Static-thrust performance. Comparison of theory, balance data, and integrated pressure data.

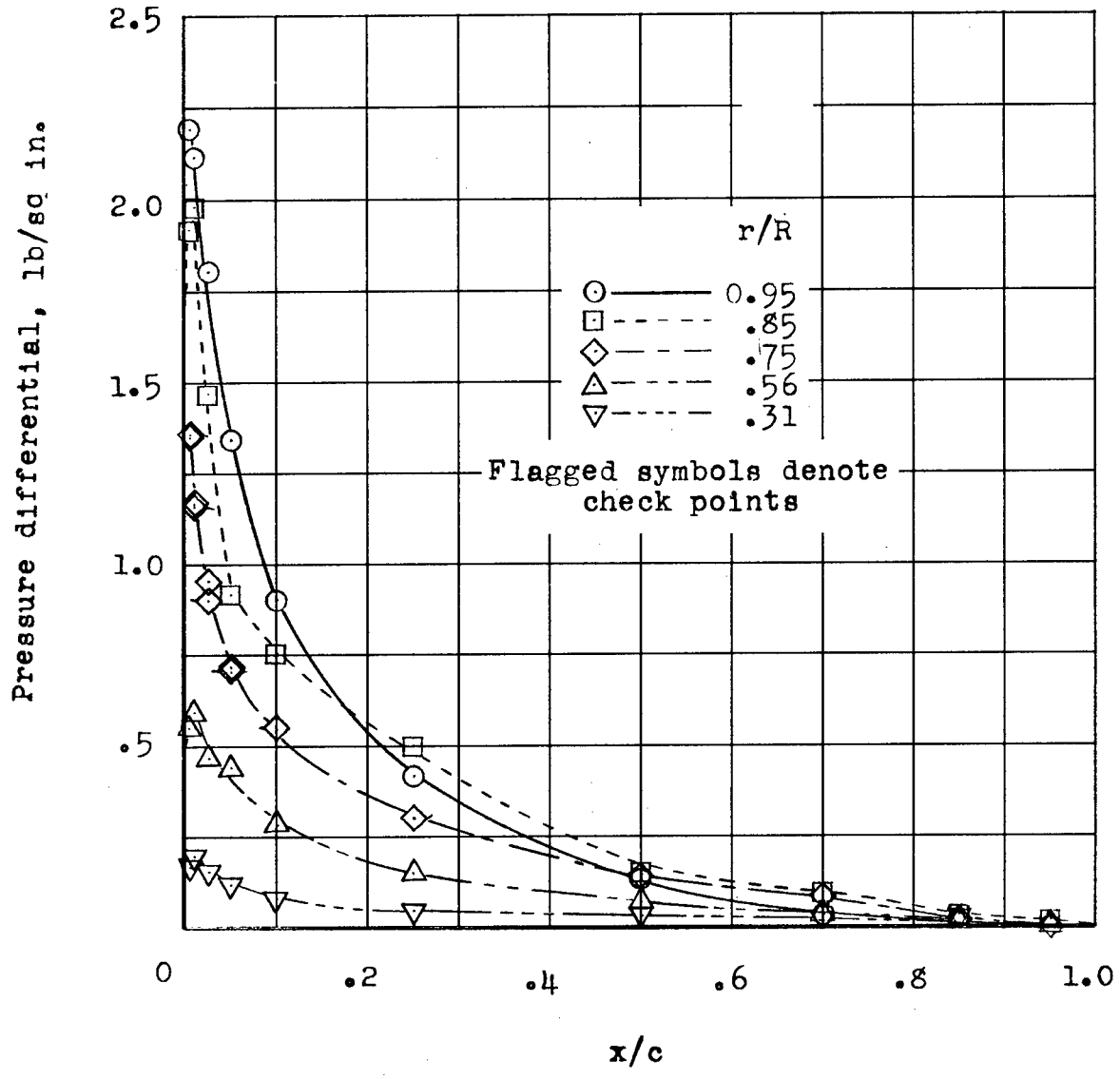

(a) ΩR = 402 ft/sec; θ = 8.9°.

Figure 6.- Representative chordwise pressure distributions for several radial stations.

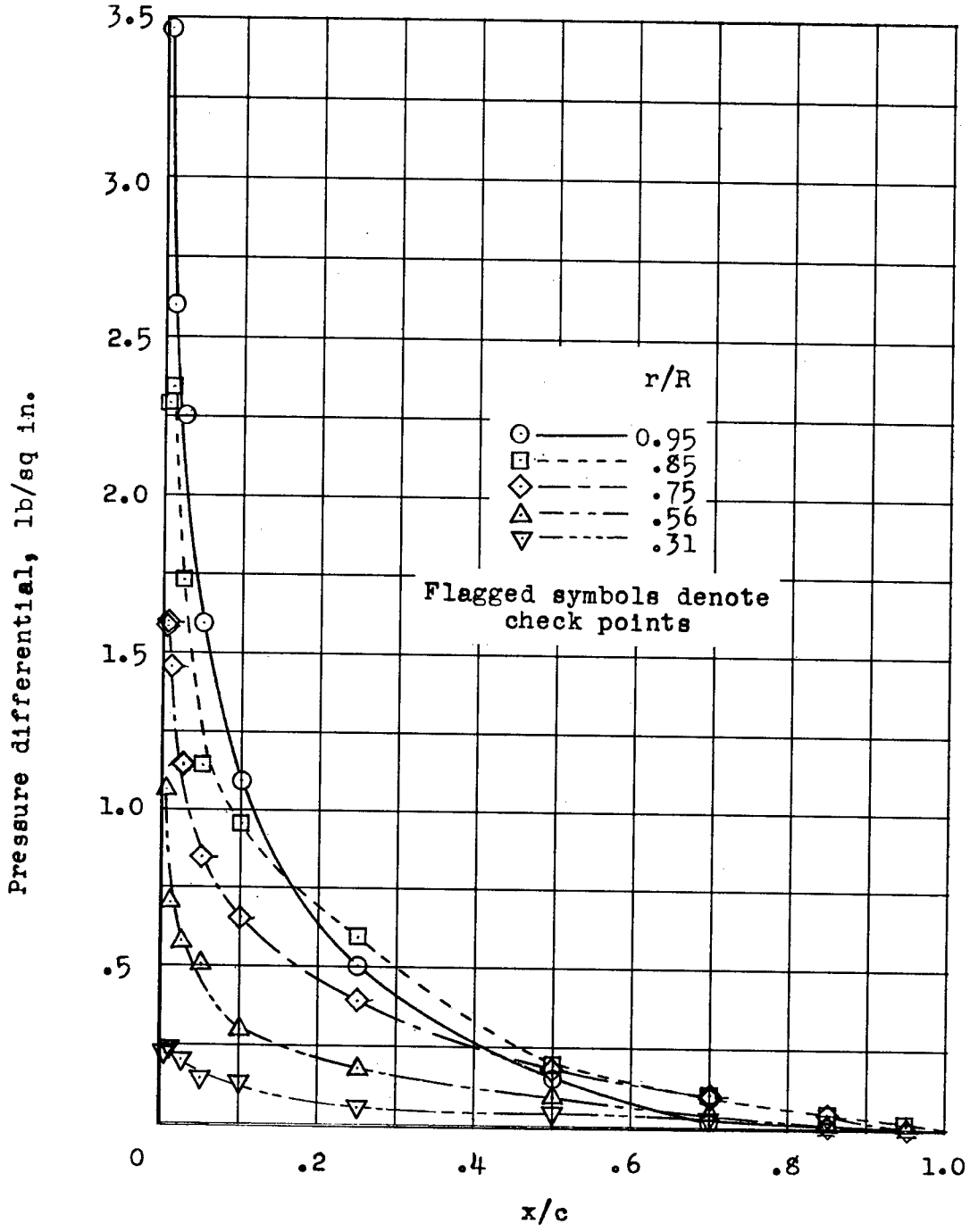

(b) ΩR = 452 ft/sec; $\theta = 8.8^{\circ}$.

Figure 6.- Continued.

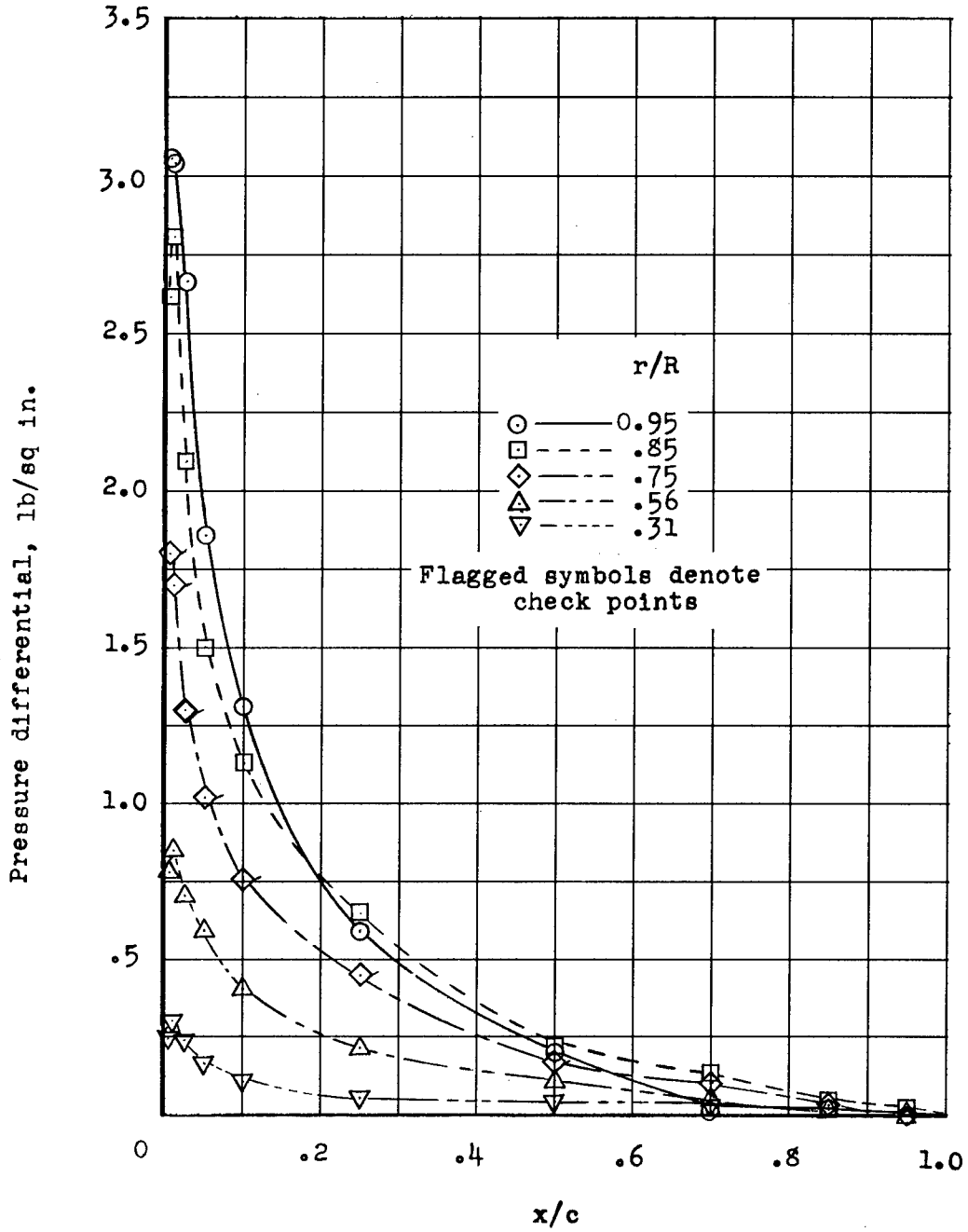

(c) ΩR = 496 ft/sec; $\theta = 8.5^{\circ}$.

Figure 6.- Concluded.

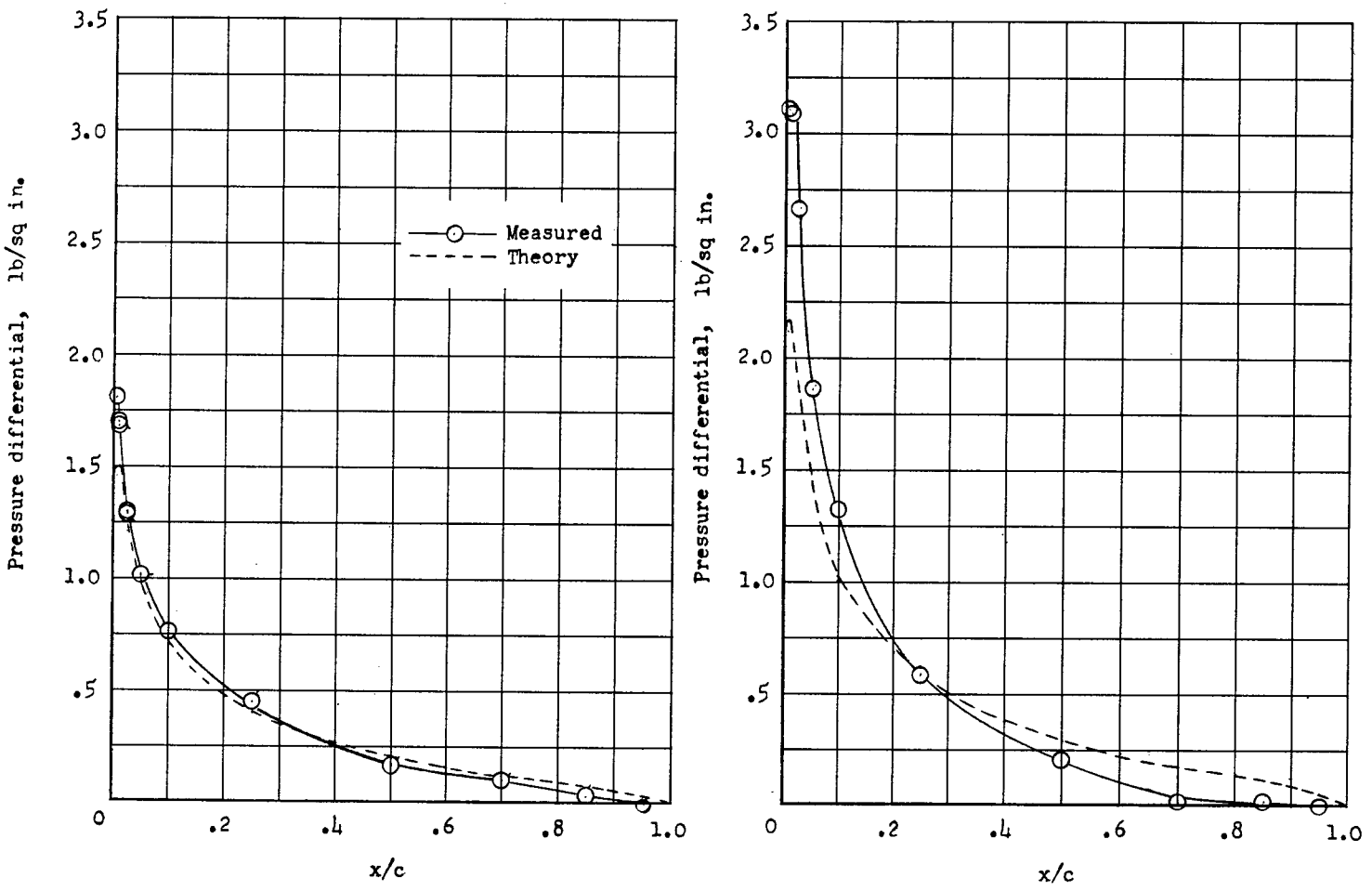

(a) $r/R = 0.75$; $C_l = 0.294$.

(b) $r/R = 0.95$; $C_l = 0.264$.

Figure 7.- Comparison of measured and theoretical chordwise loading at same lift coefficient for two radial locations. $\Omega R = 496$ ft/sec; $\theta = 8.5^\circ$.

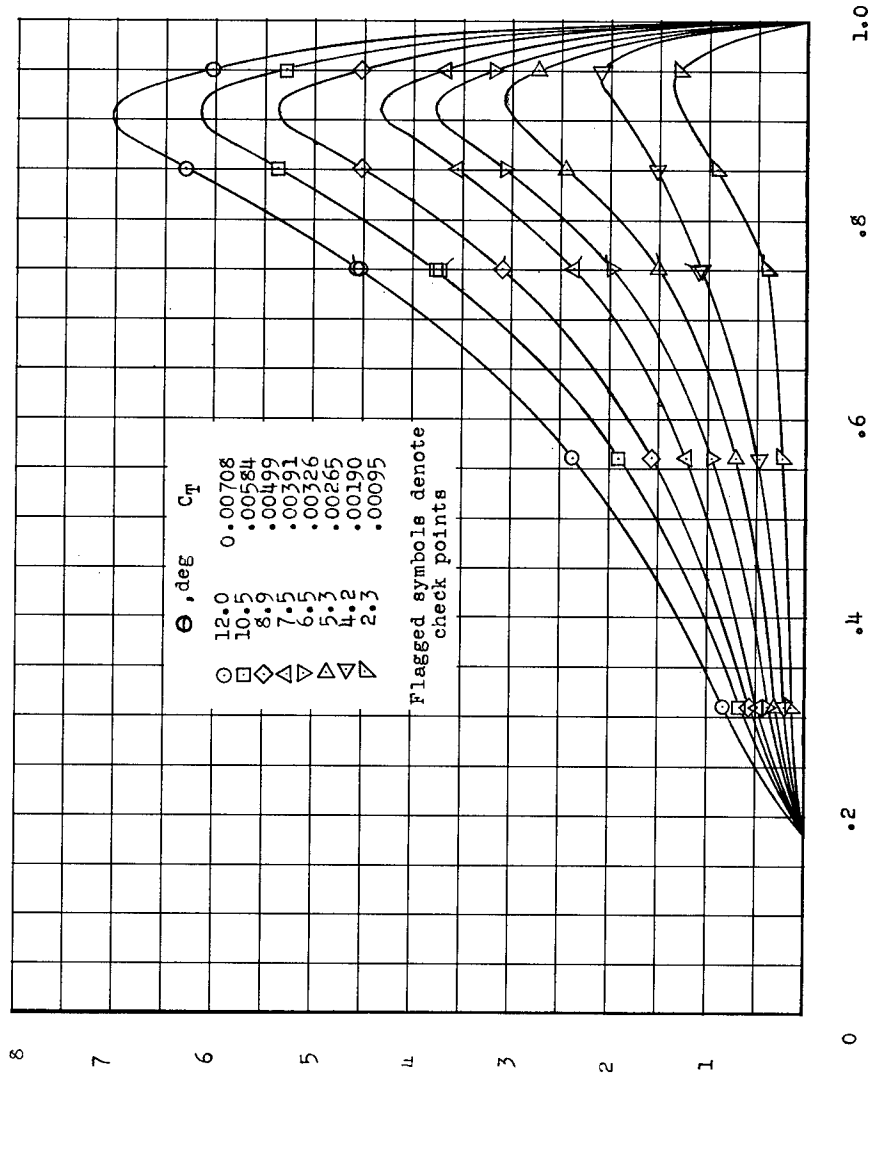

(a) ΩR = 402 ft/sec.

Figure 8.- Spanwise aerodynamic loading at various blade pitch angles.

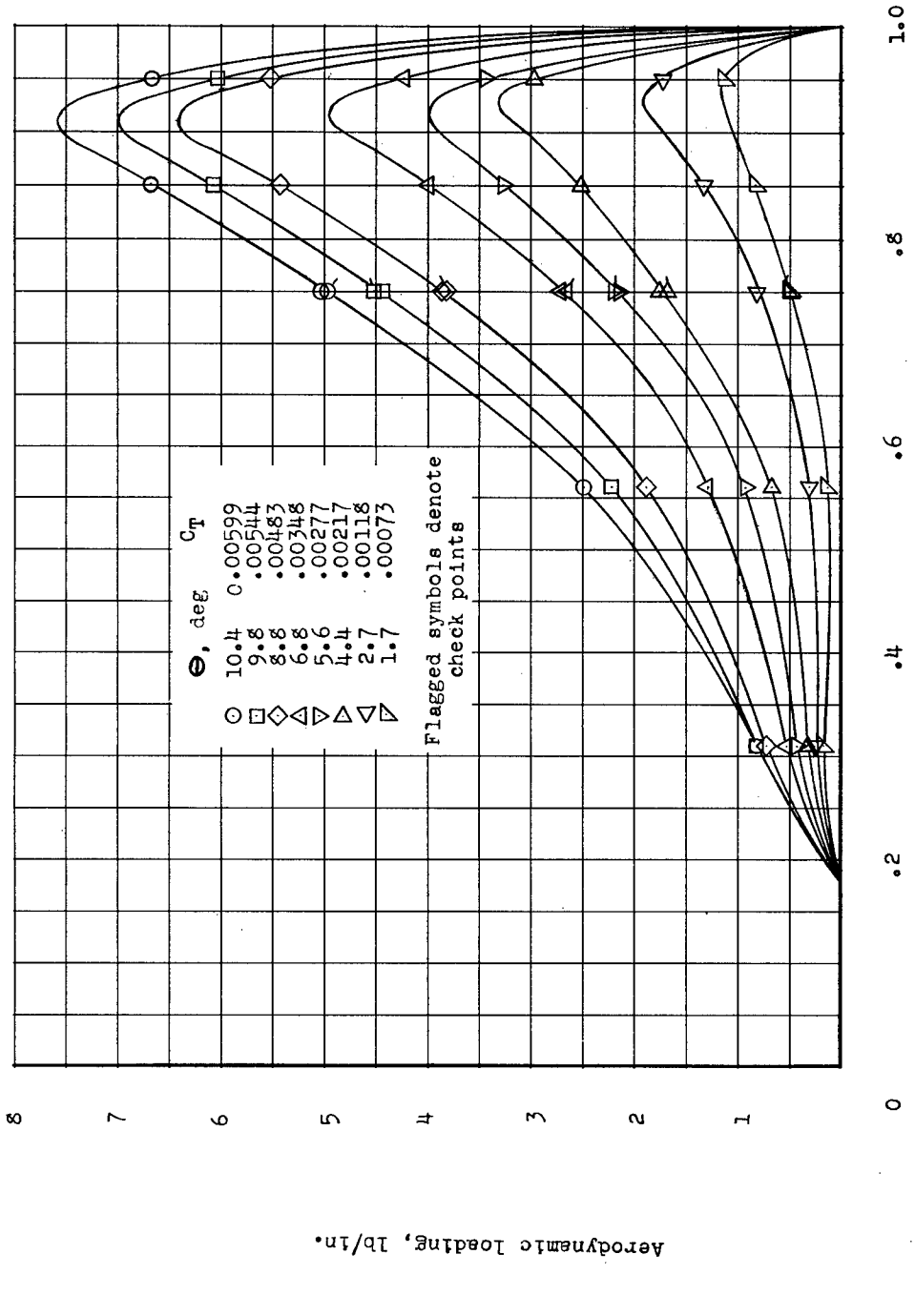

(b) ΩR = 452 ft/sec.

Figure 8.- Continued.

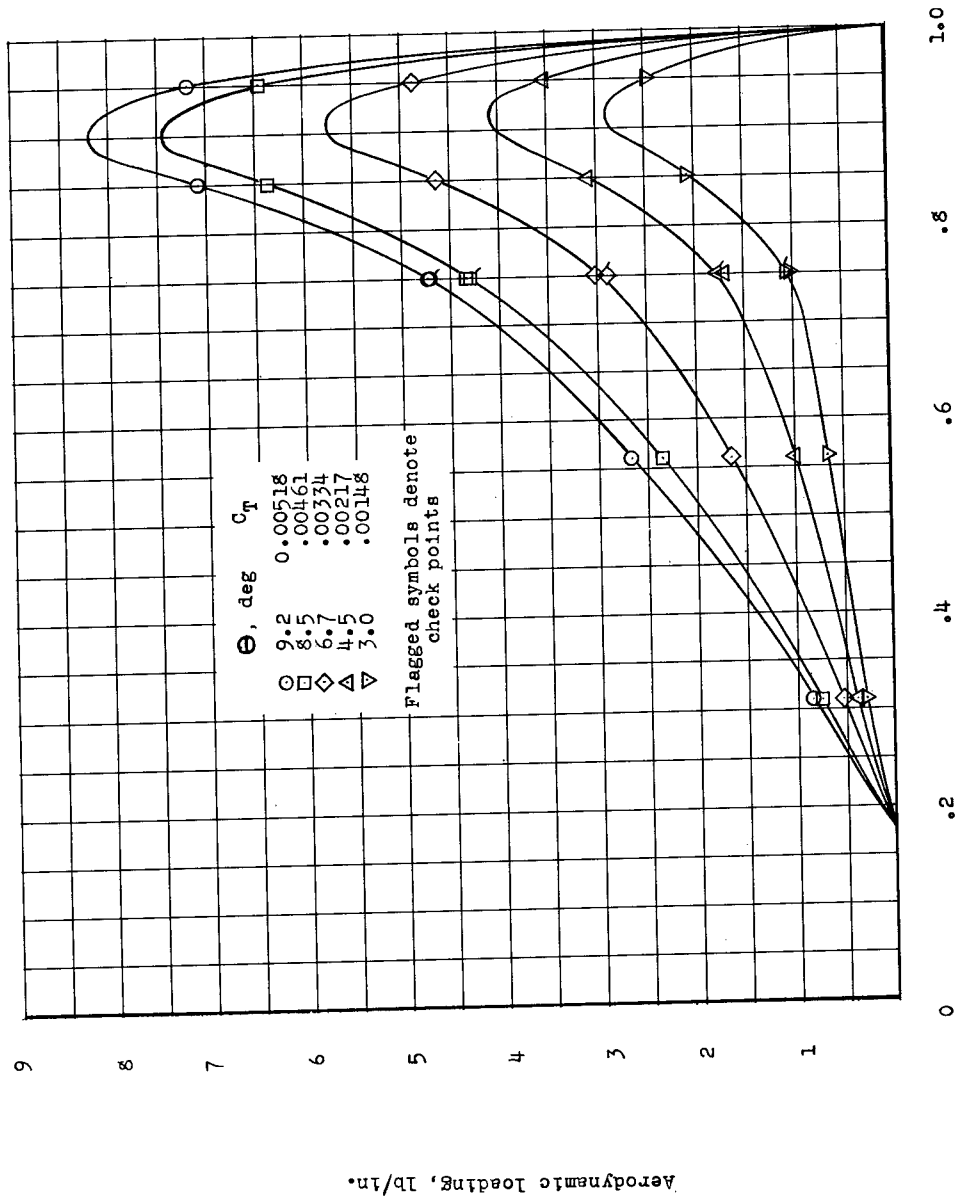

(c) ΩR = 496 ft/sec.

Figure 8.- Concluded.

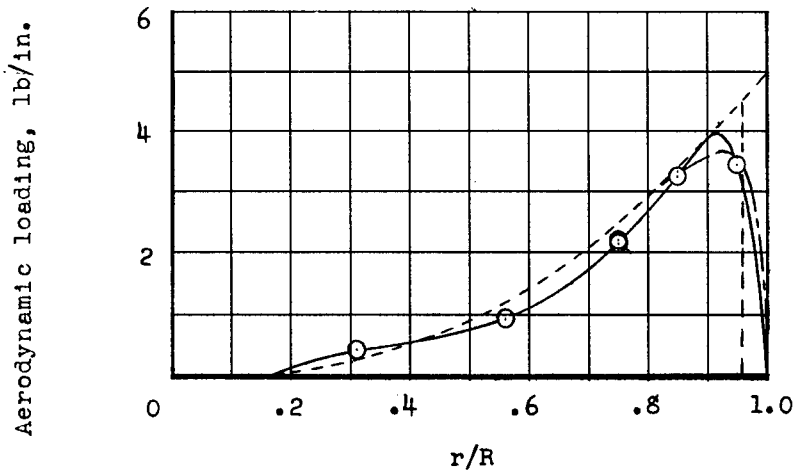

(a) ΩR = 452 ft/sec; θ = 5.6°; C_T = 0.00277.

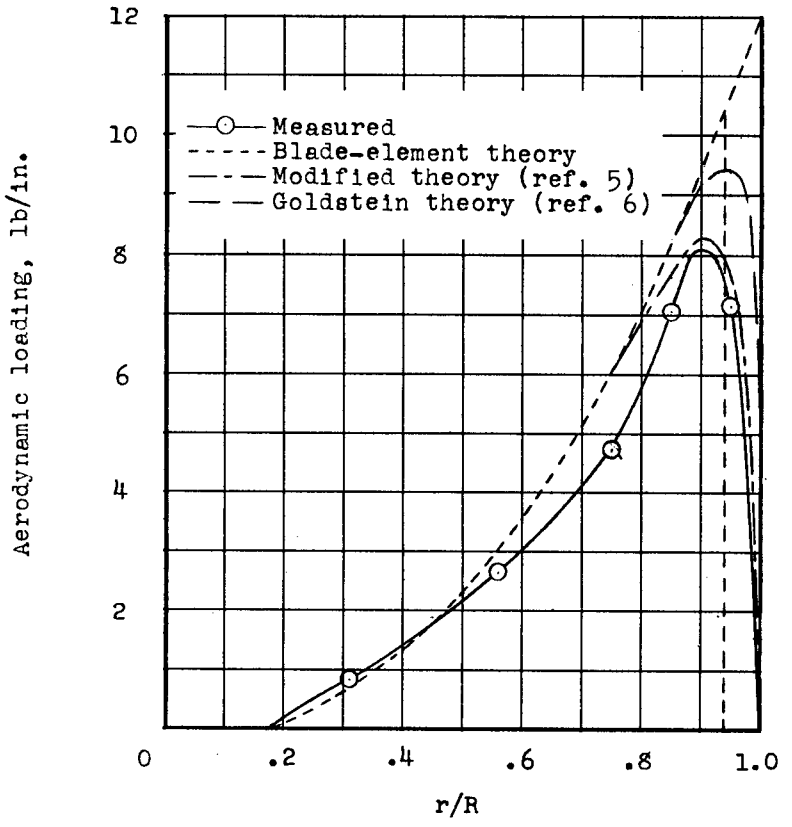

(b) ΩR = 496 ft/sec; θ = 9.2°; C_T = 0.00518.

Figure 9.- Comparison of theoretical and measured spanwise aerodynamic loading.

NACA TN 3688
National Advisory Committee for Aeronautics.
STATIC-THRUST MEASUREMENTS OF THE AERODYNAMIC LOADING ON A HELICOPTER ROTOR BLADE. John P. Rabbott, Jr. July 1956. 22p. diagrs., photos. (NACA TN 3688)

Plots of the chordwise and spanwise aerodynamic loading measured on a helicopter rotor blade in static thrust are presented. A comparison of the spanwise loading with the strip-analysis theoretical loading, as modified by a simple correction for the number of blades, shows fair agreement. The data also suggest that a tip-loss factor for performance calculations should be a function of the thrust coefficient, rather than a constant factor.

Copies obtainable from NACA, Washington

1. Wings, Rotating - Theory (1.6.1)
2. Wings, Rotating - Experimental Studies (1.6.2)
3. Helicopters (1.7.3.2)
4. Loads - Rotating Wings (4.1.1.4)

I. Rabbott, John P., Jr.
II. NACA TN 3688

NACA TN 3688
National Advisory Committee for Aeronautics.
STATIC-THRUST MEASUREMENTS OF THE AERODYNAMIC LOADING ON A HELICOPTER ROTOR BLADE. John P. Rabbott, Jr. July 1956. 22p. diagrs., photos. (NACA TN 3688)

Plots of the chordwise and spanwise aerodynamic loading measured on a helicopter rotor blade in static thrust are presented. A comparison of the spanwise loading with the strip-analysis theoretical loading, as modified by a simple correction for the number of blades, shows fair agreement. The data also suggest that a tip-loss factor for performance calculations should be a function of the thrust coefficient, rather than a constant factor.

Copies obtainable from NACA, Washington

1. Wings, Rotating - Theory (1.6.1)
2. Wings, Rotating - Experimental Studies (1.6.2)
3. Helicopters (1.7.3.2)
4. Loads - Rotating Wings (4.1.1.4)

I. Rabbott, John P., Jr.
II. NACA TN 3688

NACA TN 3688
National Advisory Committee for Aeronautics.
STATIC-THRUST MEASUREMENTS OF THE AERODYNAMIC LOADING ON A HELICOPTER ROTOR BLADE. John P. Rabbott, Jr. July 1956. 22p. diagrs., photos. (NACA TN 3688)

Plots of the chordwise and spanwise aerodynamic loading measured on a helicopter rotor blade in static thrust are presented. A comparison of the spanwise loading with the strip-analysis theoretical loading, as modified by a simple correction for the number of blades, shows fair agreement. The data also suggest that a tip-loss factor for performance calculations should be a function of the thrust coefficient, rather than a constant factor.

Copies obtainable from NACA, Washington

1. Wings, Rotating - Theory (1.6.1)
2. Wings, Rotating - Experimental Studies (1.6.2)
3. Helicopters (1.7.3.2)
4. Loads - Rotating Wings (4.1.1.4)

I. Rabbott, John P., Jr.
II. NACA TN 3688

NACA TN 3688
National Advisory Committee for Aeronautics.
STATIC-THRUST MEASUREMENTS OF THE AERODYNAMIC LOADING ON A HELICOPTER ROTOR BLADE. John P. Rabbott, Jr. July 1956. 22p. diagrs., photos. (NACA TN 3688)

Plots of the chordwise and spanwise aerodynamic loading measured on a helicopter rotor blade in static thrust are presented. A comparison of the spanwise loading with the strip-analysis theoretical loading, as modified by a simple correction for the number of blades, shows fair agreement. The data also suggest that a tip-loss factor for performance calculations should be a function of the thrust coefficient, rather than a constant factor.

Copies obtainable from NACA, Washington

1. Wings, Rotating - Theory (1.6.1)
2. Wings, Rotating - Experimental Studies (1.6.2)
3. Helicopters (1.7.3.2)
4. Loads - Rotating Wings (4.1.1.4)

I. Rabbott, John P., Jr.
II. NACA TN 3688

NACA TN 3688
National Advisory Committee for Aeronautics.
STATIC-THRUST MEASUREMENTS OF THE AERODYNAMIC LOADING ON A HELICOPTER ROTOR BLADE. John P. Rabbott, Jr. July 1956. 22p. diagrs., photos. (NACA TN 3688)

Plots of the chordwise and spanwise aerodynamic loading measured on a helicopter rotor blade in static thrust are presented. A comparison of the spanwise loading with the strip-analysis theoretical loading, as modified by a simple correction for the number of blades, shows fair agreement. The data also suggest that a tip-loss factor for performance calculations should be a function of the thrust coefficient, rather than a constant factor.

Copies obtainable from NACA, Washington

1. Wings, Rotating - Theory (1.6.1)
2. Wings, Rotating - Experimental Studies (1.6.2)
3. Helicopters (1.7.3.2)
4. Loads - Rotating Wings (4.1.1.4)

I. Rabbott, John P., Jr.
II. NACA TN 3688

NACA TN 3688
National Advisory Committee for Aeronautics.
STATIC-THRUST MEASUREMENTS OF THE AERODYNAMIC LOADING ON A HELICOPTER ROTOR BLADE. John P. Rabbott, Jr. July 1956. 22p. diagrs., photos. (NACA TN 3688)

Plots of the chordwise and spanwise aerodynamic loading measured on a helicopter rotor blade in static thrust are presented. A comparison of the spanwise loading with the strip-analysis theoretical loading, as modified by a simple correction for the number of blades, shows fair agreement. The data also suggest that a tip-loss factor for performance calculations should be a function of the thrust coefficient, rather than a constant factor.

Copies obtainable from NACA, Washington

1. Wings, Rotating - Theory (1.6.1)
2. Wings, Rotating - Experimental Studies (1.6.2)
3. Helicopters (1.7.3.2)
4. Loads - Rotating Wings (4.1.1.4)

I. Rabbott, John P., Jr.
II. NACA TN 3688